

Photocatalytic degradation of methylene blue dye by electrospun binary and ternary zinc and titanium oxide nanofibers

Beatrix Petrovičová ^{1, #}, Zainab Dahrouch ^{2, #}, Claudia Triolo ¹, Fabiola Pantò ³, Angela Malara ¹, Salvatore Patanè ^{4,*}, Maria Allegrini ⁵ and Saveria Santangelo ^{1,*}

¹ Dipartimento di Ingegneria Civile, dell'Energia, dell'Ambiente e dei Materiali (DICEAM), Università "Mediterranea", 89122 Reggio Calabria, Italy; beatrix.petrovicova@unirc.it (B.P.); claudia.triolo@unirc.it (C.T.); angela.malara@unirc.it (A.M.)

² Département de Génie Chimique, Laboratoire Physico-Chimie des Matériaux, Substances Naturelles et Environnement, Faculté des Sciences et Techniques de Tanger, Ancienne Route de l'Aéroport, Km 10, Ziaten. BP: 416. Tanger - Maroc; zainabdahrouch@gmail.com (Z.D.)

³ Istituto di Tecnologie Avanzate per l'Energia (ITAE) del Consiglio Nazionale delle Ricerche (CNR), 98126 Messina, Italy; fabiola.panto@ita.cnr.it (F.P.)

⁴ Dipartimento di Scienze Matematiche e Informatiche, Scienze Fisiche e Scienze della Terra (MIFT), Università di Messina, 98166 Messina, Italy

⁵ Istituto Nanoscienze-CNR and Dipartimento di Fisica "E. Fermi", Università di Pisa, Largo Bruno Pontecorvo 3, 56127 Pisa, Italy; maria.allegrini@unipi.it (M.A.)

* Correspondence: patanes@unime.it (S.P.); saveria.santangelo@unirc.it (S.S.)

Supplementary Materials

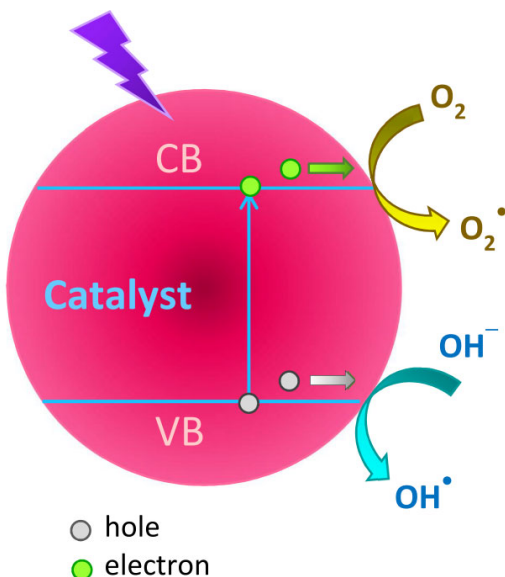


Figure S1. Sketch of the activation of the catalyst and formation of reactive radicals.

Characterization of the photocatalysts

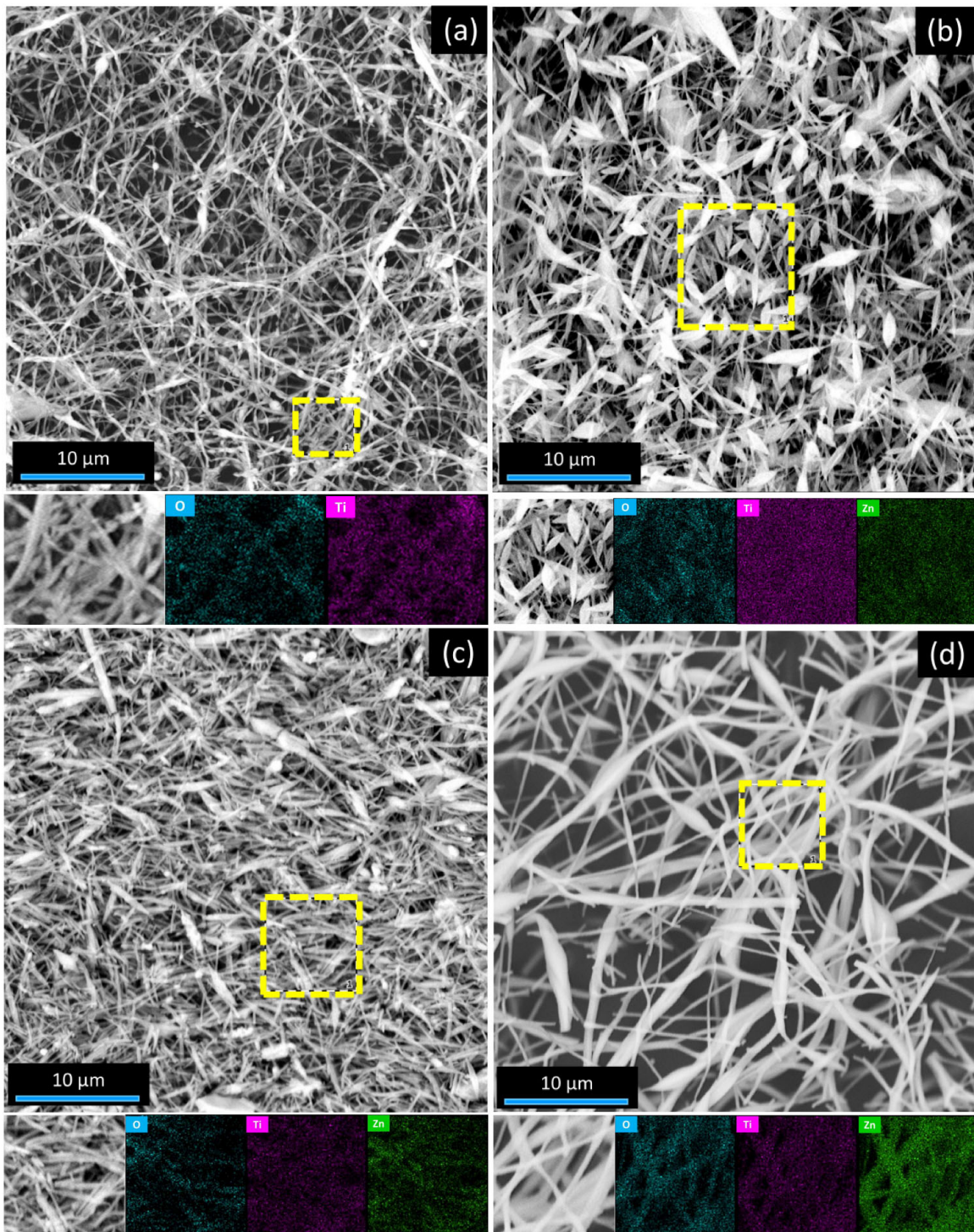


Figure S2. Results of the SEM/EDX analysis on samples (a) TZ10, (b) TZ21, (c) TZ11 and (d) TZ12.

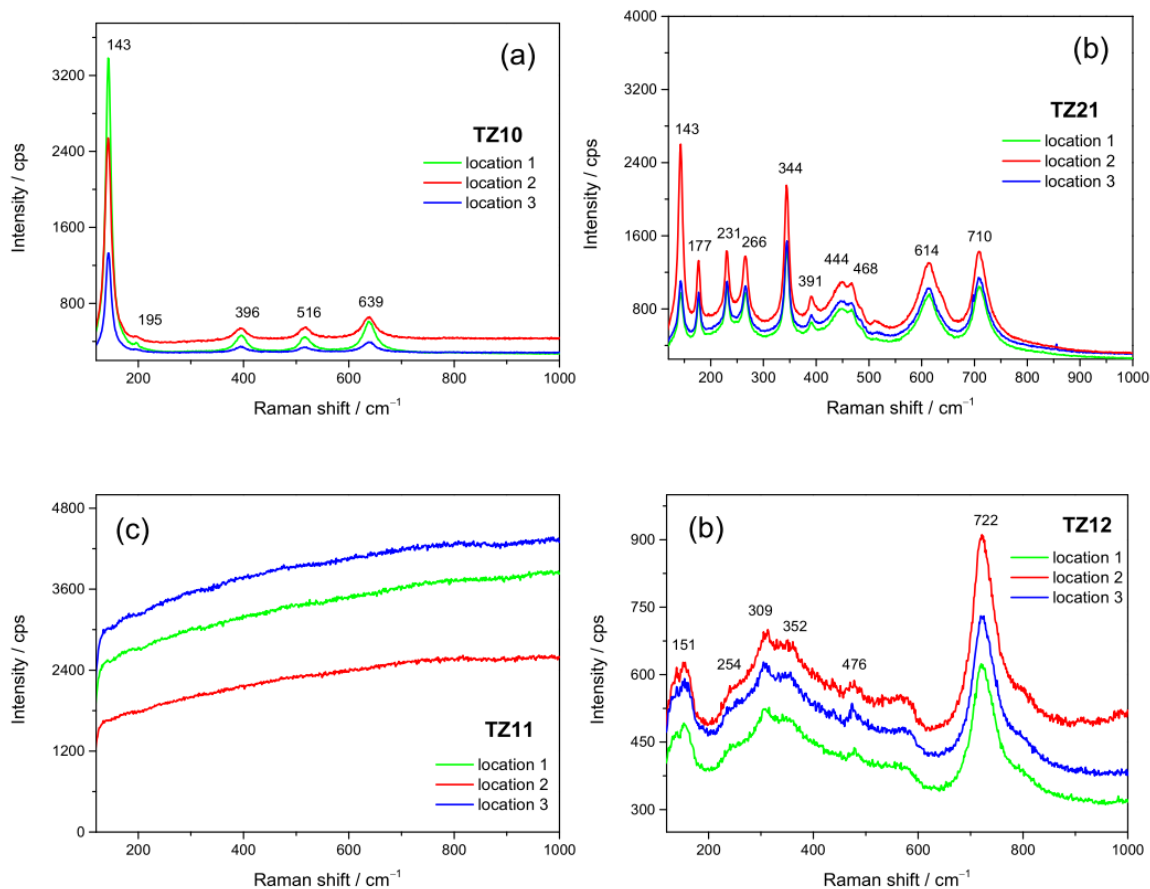


Figure S3. Micro-Raman spectra, as measured at different random locations, within each sample.

Absorbance spectrum of the dye

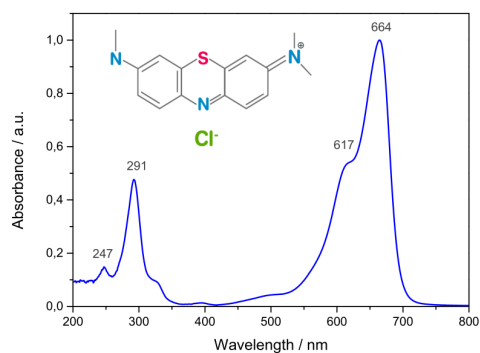


Figure S4. Absorbance spectrum of 15 μM aqueous MB solution.

Table S1. TiO₂/ZnO-based photocatalysts and their MB degradation performance.

Entry	Photocatalyst	Synthesis	Ref.	Irradiation	Catalyst concentration	Dye concentration	1h degradation percentage	<i>k</i> / min ⁻¹
1	TiO ₂	ES	[S1]	UV lamp	2.5 mg mL ⁻¹		20% (4 h)	
2	TiO ₂ /ZnO				2.5 mg mL ⁻¹		55% (4 h)	
3	TiO ₂	ES	[S2]	365 nm UV lamp	10 mg mL ⁻¹	15 μM (5mg/L)	93% (3 h)	
4	TiO ₂ /ZnO						35–83% (3 h)	
5	ZnO						99% (3 h)	
6	TiO ₂	ES	[S3]	UV lamp			68% (1.5 h)	
7	ZnO						73% (1.5 h)	
8	TZ13						85% (1.5 h)	
9	ZT21	Hydro-thermal	[S4]	Sun light (862 W cm ⁻²)	1 mg mL ⁻¹	10 μM		3.00·10 ⁻¹
10	ZT41							6.52·10 ⁻¹
11	TiO ₂ /ZnO (1:3–3:1)	Solvo-thermal	[S5]	Hg VIS lamp	2.5 mg mL ⁻¹	10 ppm	31–63% (2 h)	
12	ZnO	Hydrother mal	[S6]	Hg UV-VIS lamp (35 mW cm ⁻²)		50 μM		5.55·10 ⁻³
13	ZT12							7.46·10 ⁻³
14	ZT11							9.00·10 ⁻³
15	ZT21							1.37·10 ⁻²
16	TiO ₂							5.16·10 ⁻³
17	TiO ₂	ES	Present work	350 nm UV lamp (10 mW cm ⁻²)	0.10 mg mL ⁻¹ 0.33 mg mL ⁻¹ 0.66 mg mL ⁻¹ 1.00 mg mL ⁻¹	15 μM	94% (< 4 h) 99% (40 min) 97% (< 2 h) 99% (< 2 h)	1.24·10 ⁻² 1.12·10 ⁻¹ 3.32·10 ⁻² 4.37·10 ⁻²
18								
19								
20								
21	TZ11	ES	Present work	350 nm UV lamp (10 mW cm ⁻²)	0.33 mg mL ⁻¹	15 μM	12% (2 h)	
22	TZ12						41% (2 h), 59% (3 h)	
23	TZ21						42% (2 h), 56% (3 h)	
24	TZ21+NaOH						51% (2 h), 61% (3 h)	
25	TZ12	ES	Present work	550 nm VIS lamp (7 mW cm ⁻²)	0.33 mg mL ⁻¹	15 μM	3% (~1.5 h)	
26	TZ21+NaOH						14% (3 h)	

27	ZnO	ES	[S7]	350 nm UV lamp (10 mW cm ⁻²)	0.10 mg mL ⁻¹ 1.00 mg mL ⁻¹	15 μM	89% (< 1.5 h) 90% (< 0.5 h)	2.86·10 ⁻² 6.06·10 ⁻²
28	ZnO							
29	ZnO	ES	Present work	350 nm UV lamp (10 mW cm ⁻²)	0.33 mg mL ⁻¹ 0.66 mg mL ⁻¹	15 μM	97% (< 1.5 h) 99% (< 1 h)	4.96·10 ⁻² 7.94·10 ⁻²
30	ZnO							
31	OMTNF (TiO ₂)	ES	[S8]	UV lamp	0.17 mg mL ⁻¹	10 μM		3.84·10 ⁻²
32	TiO ₂	ES	[S9]	W UVC lamp	0.5 mg mL ⁻¹	10 ppm (~30 μM)		4.10·10 ⁻²
33	Solid TiO ₂	Humid-ES	[S10]	UV lamp	0.8 mg mL ⁻¹	10 ppm (~30 μM)		6.00·10 ⁻²
34	Porous TiO ₂							8.00·10 ⁻²
35	P25-TiO ₂ @PVDF/PVP-	ES	[S11]	365 nm UVA lamp	4x5 cm ² /50mL	10 μM		5.02·10 ⁻²

Characterization of the chemically etched photocatalyst

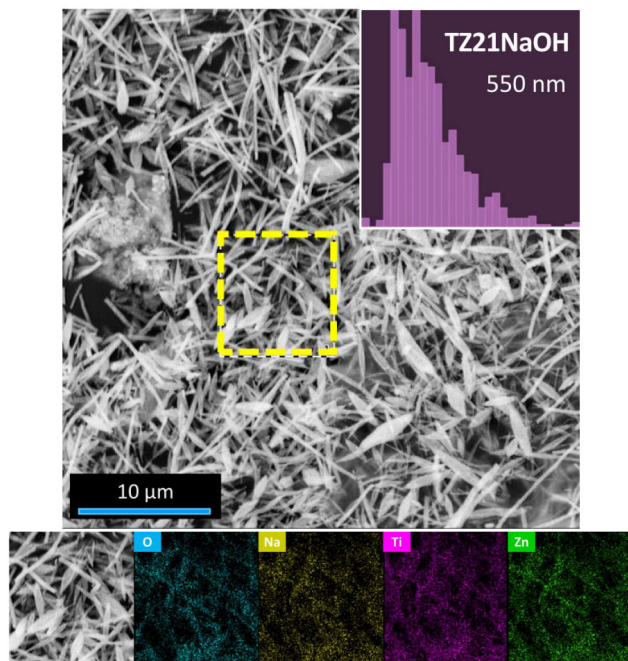


Figure S5. Results of the SEM/EDX analysis on sample TZ21NaOH.

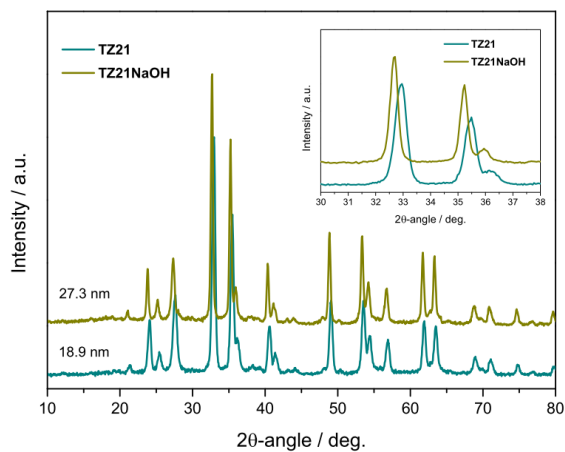


Figure S6. Results of XRPD analysis on sample TZ21 before and after chemical etching by NaOH (inset: the most intense diffraction peaks).

UV and VIS-light catalyzed degradation of the dye

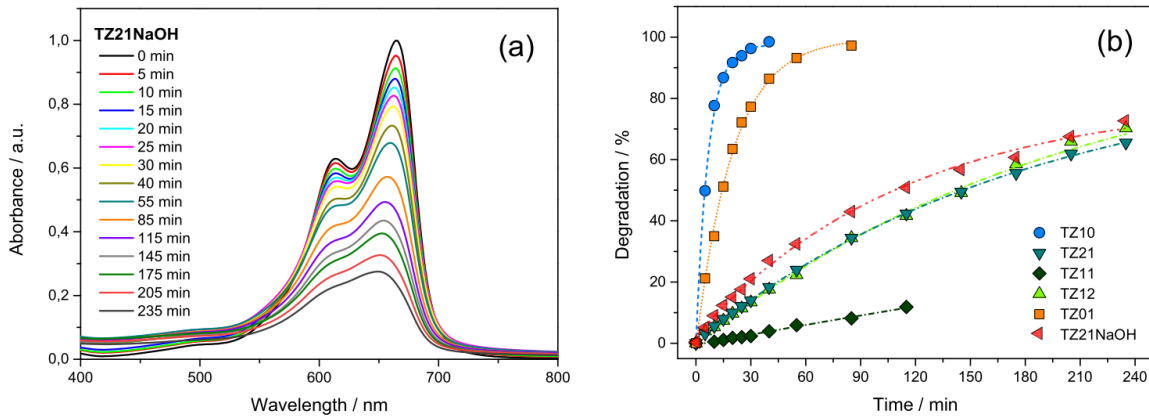


Figure S7. (a) Absorbance spectra recorded at different time intervals on an aqueous MB solution with initial 15 μM concentration, under exposure to 350 nm UV radiation (power density: 10 mW cm^{-2}) and with a catalyst concentration of 0.33 mg mL^{-1} . The shown spectra refer to photocatalyst TZ21NaOH. (b) Time-evolution of the corresponding degradation rate compared to those of un-etched photocatalysts.

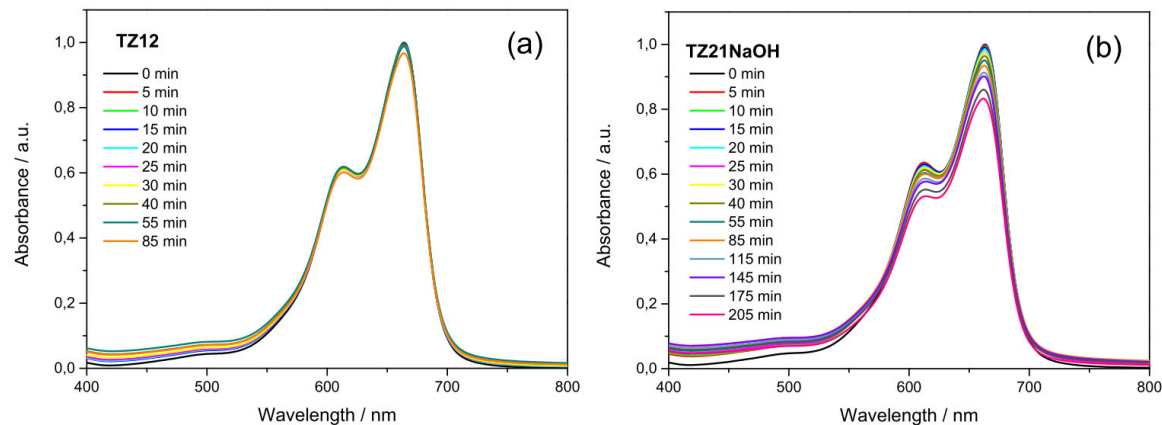


Figure S8. (a) Absorbance spectra recorded at different time intervals on an aqueous MB solution with initial 15 μM concentration, under exposure to 550 nm VIS radiation (power density: 7 mW cm^{-2}) and with a catalyst concentration of 0.33 mg mL^{-1} . The shown spectra refer to photocatalysts (a) TZ12 and (b) TZ21NaOH.

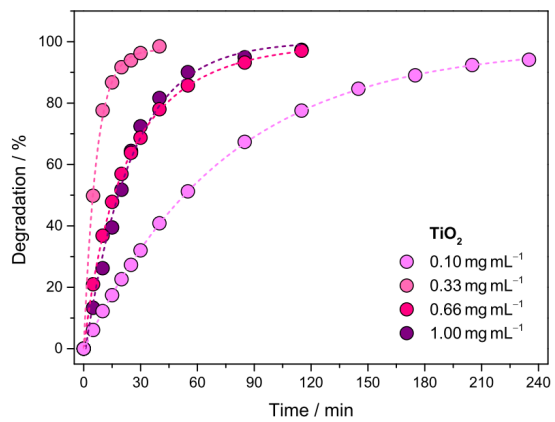


Figure S9. Time-evolution of the degradation rates under exposure to 350 nm UV radiation (power density: 10 mW cm⁻²) for different loads of α -TiO₂ NFs (photocatalyst TZ10).

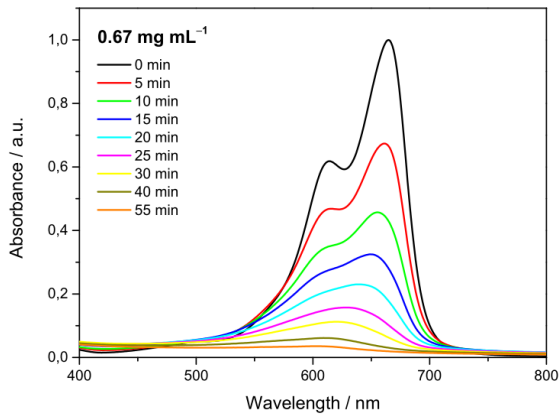


Figure S10. Absorbance spectra recorded at different time intervals on an aqueous MB solution with initial 15 μM concentration, under exposure to 350 nm UV radiation and with ZnO NFs (photocatalyst TZ01).

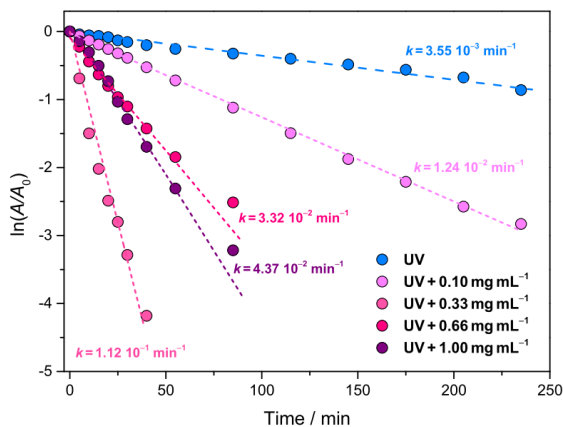


Figure S11. Semi-logarithmic plot of A_t/A_0 ratio as a function of irradiation time both without and with catalyst. The shown data refer to photocatalyst TZ10 (a -TiO₂ NFs).

Properties of the performing photocatalyst

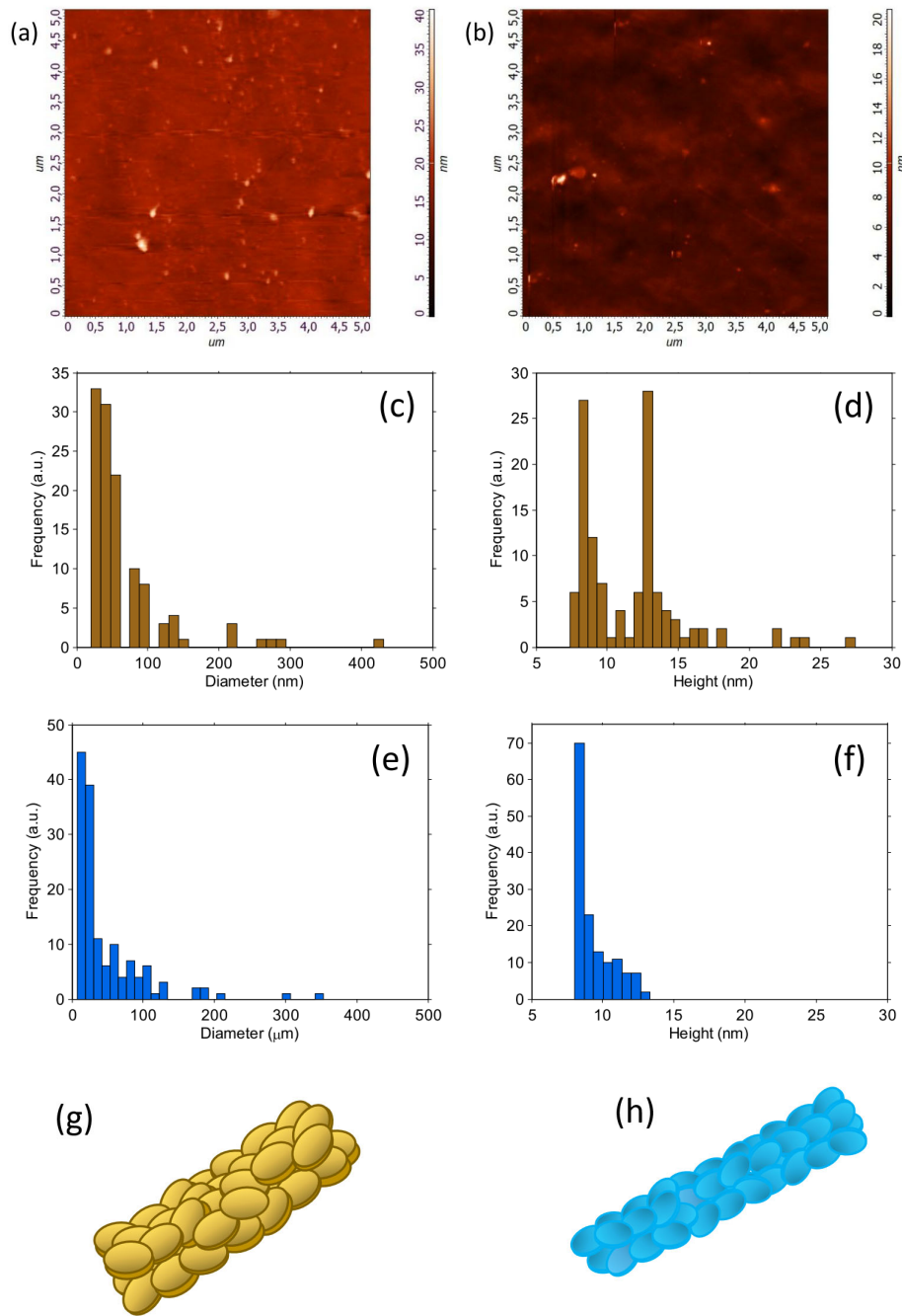


Figure S12. (a–b) Representative AFM images of NF-composing nanoparticles in sample TZ10. (c,e) Diameter and (d,f) height distributions of the NF-composing NPs and (g,h) sketch of the resulting NF architecture in samples (c,d,g) TZ10 and (e,f,h) TZ01.

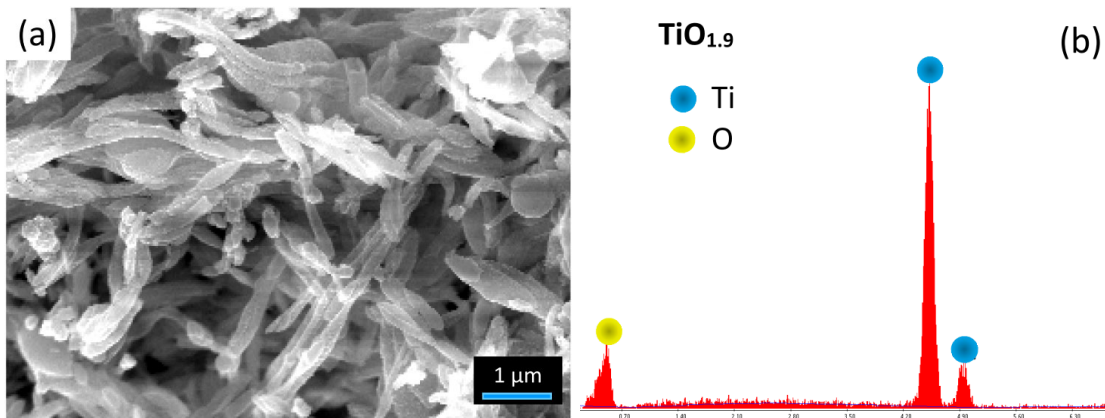


Figure S13. (a) High magnification SEM image and (b) SEM/EDX spectrum of sample TZ10.

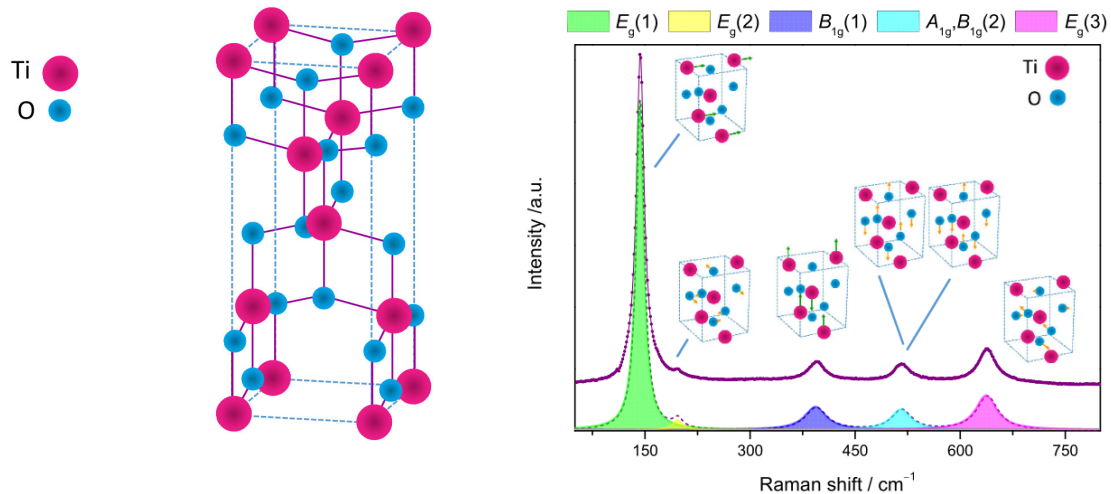


Figure S14. Anatase structure (left) and fit to the micro Raman spectrum of sample TZ10 (right; the moving ions are also indicated for each phonon mode).

Table S2. Results of the fitting procedure for the micro-Raman spectrum of sample TZ10.

Phonon mode	$E_g(1)$	$E_g(2)$	B_{1g}	$A_{1g}-B_{1g}$	$E_g(3)$
Peak frequency / cm^{-1}	143.2	194.5	395.5	516.6	638.7
FWHM / cm^{-1}	13.7	16.2	37.7	34.4	37.2

Reusability of the best performing photocatalyst

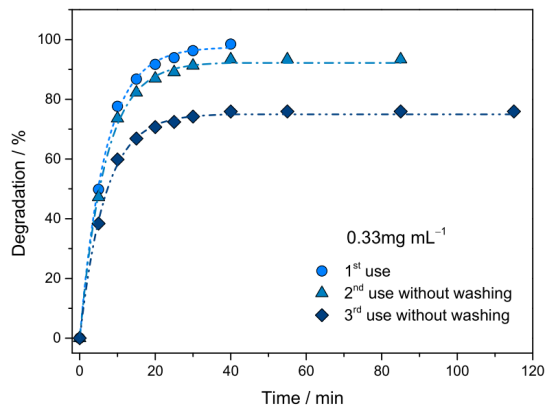


Figure S15. Reusability test for α -TiO₂ NFs (photocatalyst TZ10) under optimal load conditions (0.33 mg mL⁻¹).

References

- [S1] Lee, C. G.; Na, K. H.; Kim, W. T.; Park, D. C.; Yang, W. H.; Choi, W. Y. TiO₂/ZnO nanofibers prepared by electrospinning and their photocatalytic degradation of methylene blue compared with TiO₂ nanofibers. *Appl. Sci.* **2019**, *9*, 3404. <https://doi.org/10.3390/app9163404>.
- [S2] Kim, W. T.; Na, K. H.; Park, D. C.; Yang, W. H.; Choi, W. Y. Photocatalytic Methylene Blue Degradation of Electrospun Ti-Zn Complex Oxide Nanofibers. *Nanomaterials* **2020**, *10*, 1311. <https://doi.org/10.3390/nano10071311>.
- [S3] Someswararao, M. V.; Dubey, R. S.; Subbarao, P. S. V. Electrospun composite nanofibers prepared by varying concentrations of TiO₂/ZnO solutions for photocatalytic applications. *J. Photochem. Photobiol. A* **2021**, *6*, 100016. <https://doi.org/10.1016/j.jpap.2021.100016>.
- [S4] Singh, J.; Kumar, S.; Manna, A. K.; Soni, R. K. Fabrication of ZnO-TiO₂ nanohybrids for rapid sunlight driven photodegradation of textile dyes and antibiotic residue molecules. *Opt. Mater.* **2020**, *107*, 110138. <https://doi.org/10.1016/j.optmat.2020.110138>.
- [S5] Mohamadi Zalani, N.; Koozegar Kaleji, B.; Mazinani, B.; Synthesis and characterisation of the mesoporous ZnO-TiO₂ nanocomposite; Taguchi optimisation and photocatalytic methylene blue degradation under visible light. *Materials Technology* **2020**, *35*(5), 281-289. <https://doi.org/10.1080/10667857.2019.1678087>.
- [S6] Chen, D.; Zhang, H.; Hu, S.; Li, J. Preparation and enhanced photoelectrochemical performance of coupled bicomponent ZnO-TiO₂ nanocomposites. *J. Phys. Chem. C* **2008**, *112*, 117-122. <https://doi.org/10.1021/jp077236a>.
- [S7] Pantò, F.; Dahrouch, Z.; Saha, A.; Patanè, S.; Santangelo, S.; Triolo, C. Photocatalytic degradation of methylene blue dye by porous zinc oxide nanofibers prepared via electrospinning: When defects become merits. *Appl. Surf. Sci.* **2021**, *557*, 149830. <https://doi.org/10.1016/j.apsusc.2021.149830>.
- [S8] Chattopadhyay, S.; Saha, J.; De, G. Electrospun anatase TiO₂ nanofibers with ordered mesoporosity. *J. Mater. Chem. A* **2014**, *2*, 19029-19035. <https://doi.org/10.1039/C4TA04481A>
- [S9] Soo, J. Z.; Lee, K. M.; Ang, B. C.; Ong, B. H. Optimal electrospun TiO₂ nanofiber photocatalytic performance via synergistic morphology and particle crystallinity with anatase/rutile phase tuning. *Phys. Status Solidi (a)* **2019**, *216*, 1900066. <https://doi.org/10.1002/pssa.201900066>

[S10] Aghasiloo, P.; Yousefzadeh, M.; Latifi, M.; Jose, R. Highly porous TiO₂ nanofibers by humid-electrospinning with enhanced photocatalytic properties. *J. Alloys Comp.* **2019**, *790*, 257–265. <https://doi.org/10.1016/j.jallcom.2019.03.175>

[S11] Lee, C. G.; Javed, H.; Zhang, D.; Kim, J.H.; Westerhoff, P.; Li, Q.; Alvarez, P. J. J. Porous Electrospun Fibers Embedding TiO₂ for Adsorption and Photocatalytic Degradation of Water Pollutants. *Environ. Sci. Technol.* **2018**, *52*, 4285–4293. <https://doi.org/10.1021/acs.est.7b06508>